# Electronic polarization effects in core-level spectroscopy

Iskander Mukatayev, Gabriele d'Avino, Benoit Sklenard, Valerio Olevano, Jing Li

# Polarization Induced Core-Level Shift in Noble Gas Clusters by Embedded Many-Body Perturbation Theory

Iskander Mukatayev,[1] Gabriele D'Avino,[2,3] Benoît Sklénard,[1,4] Valerio Olevano,[2,3,4,*] and Jing Li[1,4,†]

[1] *Université Grenoble Alpes, CEA, Leti, F-38000, Grenoble, France*
[2] *Université Grenoble Alpes, F-38000 Grenoble, France*
[3] *CNRS, Institut Néel, F-38042 Grenoble, France*
[4] *European Theoretical Spectroscopy Facility (ETSF), F-38000 Grenoble, France*

(Dated: April 28, 2023)

In X-ray photoelectron spectroscopy (XPS), the excited orbital interact with its polarized charges, resulting in a lower binding energy. Demonstration by an embedded many-body theory, such polarization effect can shift the core-level energy more than 1 eV in noble gas clusters made of Ar, Kr, or Xe. The polarization energy is almost identical for any core-orbitals within an atom but significantly depends on the atomic position in the cluster. An analytical formula is derived from classical electrostatics and can describe such a phenomenon well. The simulated XPS spectra agree with experiments of noble gas clusters consisting of 3000 atoms. The polarization energy is another important contributor compared to the crystal field to the core-level shift.

*Introduction.* — X-ray photoelectron spectroscopy (XPS) measures the binding energy of core-electron by evaluating the kinetic energies of emitted electrons under the action of X-rays [1, 2]. It provides the chemical composition of any samples, i.e., atoms, molecules, liquids, solids, crystalline, or amorphous. In addition, it allows access to structural information, such as chemical bondings and local structures, through the core-level shift, the change in the binding energy of a core electron. However, it requires established knowledge, which associates the chemical bonding to core-level shift. While such knowledge might be acquired experimentally, for example, the rich chemical bondings of the carbon atom are tabulated, a more promising way is to develop an accurate method to simulate core-level shift for any species in any environment.[3]

The recent introduction of many-body theory to the simulation of XPS spectra improves the accuracy of the absolute value of core-level energies.[4–8] The computed XPS peaks of noble gas atoms from He to Rn with binding energy up to 100 keV are comparable to experiments typically with an error below 1%.[4] The accuracy is also validated in a set of small molecules containing light elements, such as C, N, O, and F atoms[5, 6]. The fragmented approach could be an efficient method for large molecules and polymers.[7] However, the core-level shift deserves more attention than only focusing on the absolute value of XPS peaks. The previous work on carbon 1s demonstrated that the main effect of the core-level shift originated from classical electrostatics [8], which contains the the crystal field, characterized by the electrostatic potential brought by surrounding atoms, and the polarization effect due to the core-level excitation by the X-ray. The crystal field is typically captured accurately and efficiently by density functional theory (DFT) or the Hartree-Fock (HF) approach. The dynamic part requires more complex methods such as ΔSCF or many-body theory. The screening effect of core-level exciting among small gas-phase molecules is similar, which justifies the evaluation of core-level shift directly in DFT or HF for a set of gas-phase molecules. [8]

Nevertheless, the polarization effect would dominate the core-level shift in some conditions. For example, when applying the fragmented *GW* approach, attention has to be paid to the change in the dielectric environment, which might underestimate the polarization energy. To demonstrate the polarization effect on core-level shift, we choose noble gas clusters as an example, which is ideal. Because they are formed by van der Waals interactions, noble gas clusters have almost no crystal field effect. Therefore, different peaks in experimental XPS spectra must be ascribed to the change of polarization energy for atoms on the surface and in bulk. [9, 10] However, many questions remain. Does the polarization effect depend on which orbital is excited? Does it depend on the crystallography orientation? In this letter, we employed the embedded many-body perturbation theory to systematically investigate the polarization effect on core-level shifts in noble gas clusters.

*Methods.* — The core-electron excitation of a noble gas atom in a cluster is computed within an embedded many-body perturbation theory implemented in the quantum mechanic / molecular mechanic (QM/MM) approach [11, 12]. The *GW* method models the QM part by constructing the one-body Green's function

$$G(r,r';\omega)=\sum_n \frac{\psi_n(r)\psi_n^\dagger(r')}{\omega-\epsilon_n+i\eta\,\mathrm{sgn}(E_n-\mu)}, \qquad (1)$$

where $\psi$ and $E$ are wave functions and energies of eigenstates, $\mu$ the chemical potential, and $\eta$ positive infinitesimal number; followed by the random-phase approximation polarizability,

$$\chi_0(r,r';\omega) = \sum_{i,j} (f_i - f_j) \frac{\psi_i^\dagger(r)\psi_j(r)\psi_j^\dagger(r')\psi_i(r')}{E_i - E_j - \hbar\omega + i\eta\,\mathrm{sgn}(E_i - E_j)}, \tag{2}$$

where $f$ is the occupation number. The dynamically screened Coulomb potential is

$$W(r,r';\omega) = w(r,r') + \int dr_1 dr_2 w(r,r_1)\chi_0(r_1,r_2;\omega)W(r_2,r';\omega) \tag{3}$$

where $w$ is the effective Coulomb potential in the QM part. In conventional $GW$ without embedding, $w$ is simply the bare Coulomb potential $v$. With embedding, $w$ includes the screening effect from the MM part, i.e.,

$$w(r,r') = v(r,r') + \int dr_1 dr_2 v(r,r_1)\chi^{MM}(r_1,r_2)W(r_2,r'), \tag{4}$$

where $\chi^{MM}$ is the polarizability in the MM part. The second term in Eq.4 is called the reaction field matrix. Finally, the $GW$ self-energy is obtained

$$\Sigma(r,r';\omega) = \frac{i\hbar}{2\pi}\int d\omega' G\left(r,r',\omega+\omega'\right) W(r,r',\omega) \tag{5}$$

The $GW$ quasi-particle energy is a solution of the following quasi-particle equation based on the perturbation theory by replacing the exchange-correction potential in DFT with the self-energies.

$$E_n^{GW} = \epsilon_n^{KS} + \langle\phi_n^{KS}|\Sigma(E_n^{GW}) - V_{XC}^{DFT}|\phi_n^{KS}\rangle \tag{6}$$

The polarization energy from the MM part is the difference between quasi-particle energies with and without embedding.

$$P_n = \sigma_n(E_n^{GW/MM} - E_n^{GW}), \tag{7}$$

where $\sigma_n = 1$ for occupied orbitals, and $-1$ for unoccupied ones.

In practice, we performed eigenvalues self-consistent $GW$ gas-phase calculation (ev$GW$) starting from Hartree-Fock (HF) eigenstates. By using the ev$GW$ quasi-particle energies, single-shot COHSEX calculations (Coulomb-hole-screened-exchange formalism, the static version of $GW$ approximation [13]), with and without the screening from the MM part, were used to evaluate the polarization energy. The error from the ignorance of frequency dependence is largely canceled by subtracting two quasi-particle energies, as demonstrated recently using the fragmented $GW$ approach, which considers the MM part's dynamical response [14].

The HF eigenstates used as starting point for $GW$ calculation were obtained using x2c-TZVPPall-2c basis set [15] with NWChem [16]. The embedded $GW$ calculations are performed using FIESTA package [11, 17, 18] with Coulomb-fitting resolution of identity technique (RI-V)[19] and def2-universal-JKFIT auxiliary basis set[20]. The MM part is described by a discrete polarizable model implemented on MESCAL package[21]. The isotropic polarizability of noble gas atoms is taken from experiments [22, 23] and was set to 1.641, 2.4844, and 4.044 $\mathring{A}^{-3}$ for Ar, Kr, and Xe, which are in face-center cubic structure with lattice parameters 5.25, 5.59, and 6.13 $\mathring{A}$, respectively.[24–26] For an atom on a semi-infinite surface or in bulk, its reaction field matrix is extrapolated from a semi-sphere or sphere to an infinite radius.[12]

*Results.* — Considering a noble gas atom in its bulk solid (sphere with infinite radius), Fig. 1 shows that the polarization energy is almost a constant for all orbitals. It is about 1.16, 1.27, and 1.35 eV for Ar, Kr, and Xe, respectively. For an atom at a surface (a semisphere with an infinite radius), the polarization energy reduces by 0.2 to 0.3 eV compared to that in bulk but remains a constant, which is 0.82, 0.92, and 1.01 eV for Ar, Kr, and Xe, respectively. The reduction of polarization energy on the surface is expected as the polarizable medium is reduced.

The orbital-independent polarization energy can be explained by the Gauss theorem. Assume the noble gas atom is in a spherical cavity with radius $r_c$, outside of which is the polarizable medium. The electric field in the polarizable medium is always $1/(\epsilon R^2)$ ($R > r_c$, where $\epsilon$ is the dielectric constant), for any core-level excitation, i.e., the shape of the orbital has no influence. Therefore, the polarizable medium has the same response to the electric field by developing dipoles. In the cavity, the electric field that arose from the polarized dipoles is zero, so the potential $V(r)$ from those dipoles is a constant. The polarization energy is simply $P = \int dr V(r)\psi^\dagger(r)\psi(r) = V$, where $\psi$ is the excited orbital.

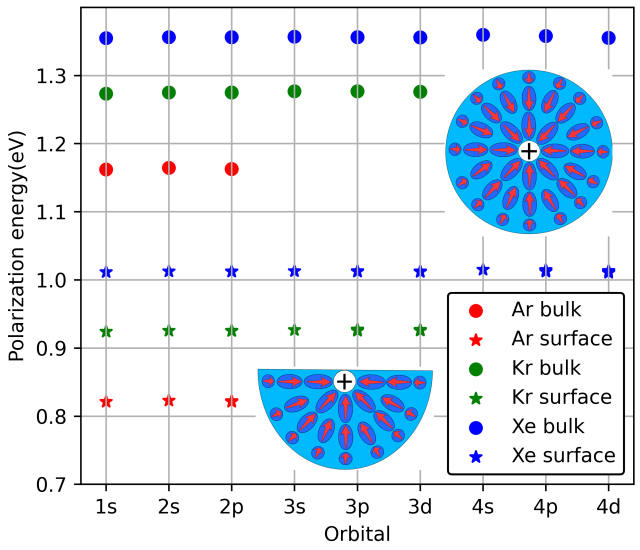


FIG. 1. Polarization energy induced core-level shift for all core orbitals of Ar, Kr, and Xe in bulk (sphere with infinite radius) and on a surface (semi-sphere with infinite radius).

In the following, we discuss finite-size clusters. The polarization energy of the atom at the cluster's center is smaller than in bulk because of the reduced polarizable medium. Considering a cluster about 3 nm in radius, the center atom has 1.06, 1.17, and 1.25 eV for Ar, Kr, and Xe, respectively, which are about 0.1 eV small than that in bulk. By moving the target atom away from the spherical center and toward the surface, the polarizable medium becomes asymmetric. Here, we consider four paths from center to surface, i.e., $\langle 001\rangle$, $\langle 011\rangle$, $\langle 111\rangle$, and $\langle 211\rangle$. Along these paths, the polarization energy is plotted as a function of the distance to the center of the sphere in Fig. 2. As expected, it decreases. This is because the volume of polarizable medium is fixed; part of the medium is further away when the target atom is off-center. Therefore, weaker electric field, smaller dipole, and reduced polarization energy. Interestingly, the path dependence is weak; only the distance to the center matters. When the target atom reaches the surface, its polarization energy is much smaller than on a semi-infinite surface due to the finite polarizable medium and convexed surface with more exposition to vacuum.

To explain the polarization energy versus distance to the center qualitatively, we developed an analytical formula. The target atom is located at a distance $r$ from the center in a cavity with radius $r_c$. The polarizable medium is a sphere with radius $R_s$ and dielectric constant $\epsilon$. According to classical electrostatics, the polarization energy has the following form (the detailed derivation is available in supplemental information)

$$P(r) = \frac{\pi\alpha}{\epsilon^2}\left[-4\left(\frac{1}{R_s - r} - \frac{1}{r_c}\right) + \frac{\left[4r^2 + 2R_s r + (R_s^2 - r^2)(\ln\{R_s - r\} - \ln\{R_s + r\})\right]}{r(R_s^2 - r^2)}\right]. \quad (8)$$

By taking the polarization energy in bulk and in the center of a finite sphere with 3000 atoms with radius $R_s$ of 31.2, 32.5, and 37.0 $\mathring{A}$ for Ar, Kr, and Xe, the dielectric constant and cavity radius are solved from Eq. 8. The dielectric constant is 1.19, 1.25, and 1.30, for Ar, Kr, and Xe, and the cavity radius is 2.48, 2.59, and 2.76 $\mathring{A}$. By using these parameters, the distance dependence is well captured by the analytical formula. For atoms on the surface, due to the discretized atomic position, the analytical formula derived from the continuous polarizable model has some deviation.

Comparing with experimental XPS spectra requires the polarization energy of any atom in a sphere, which can be quickly evaluated by the analytical formula (Eq.8), avoiding thousands of embedded *GW* calculations. Considering the decay of incident X-ray, the intensity of XPS peaks is proportional to $e^{\frac{-|r-R_s|}{\lambda}}$, where $\lambda$ is the decay length and was set to 8 $\mathring{A}$ for the three types of noble gas clusters. To focus on the polarization effect, we take the experimental peaks for atomic Ar $2p_{1/2}$, Kr $3d_{3/2}$, and Xe $4d_{3/2}$ peaks at $-250.6$, $-95.0$, and $-69.5$ eV, [27], to avoid the error on the absolute binding energy in *GW* calculation, which is generally within 1%.[8] The spin-orbital splittings were 2.1, 1.2, and 2.0 eV for Ar 2p, Kr 3d, and Xe 4d from experiment.[27]

Figure 3 shows that simulated XPS spectra agree with experiments for Ar, Kr, and Xe clusters of 3000 atoms. [9] Peaks of an isolated noble gas atom are also added to indicate the relative position to surface and bulk peaks. It is obvious that the experimental "surface" peak consists of several contributions of atoms on and close to the surface, with a range of low polarization energy. The experimental "bulk" peak is from atoms deeper in the cluster. However, the atom close to the sphere's center contributes little to the spectra due to X-ray attenuation.

*Conclusion.* — We demonstrated the strong polarization effect on core-level shift for noble gas atoms in its cluster by employing embedded many-body perturbation theory. The polarization energy is independent of which core-orbital is excited but depends on the position of the target atom in the cluster. An analytical formula derived from electrostatic capture well the position-

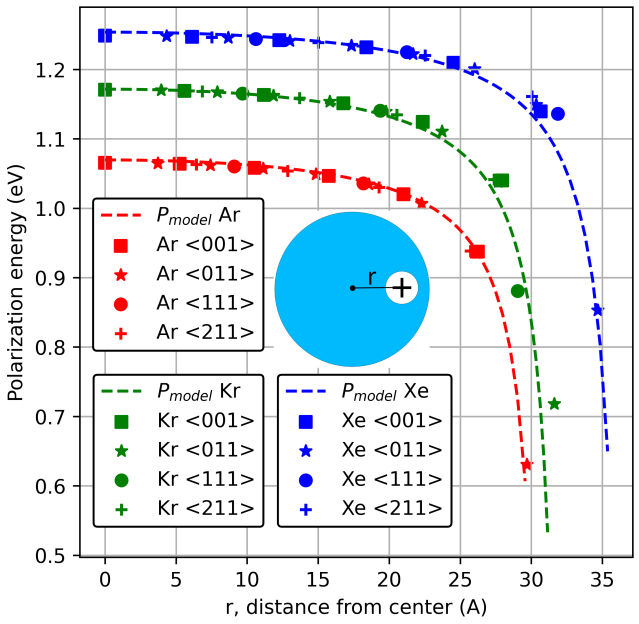


FIG. 2. Polarization energy of a target atom with the distance $r$ to the center of the cluster in four crystalline directions ($\langle 001\rangle$, $\langle 011\rangle$, and $\langle 111\rangle$), the dashed line is from the analytical formula (Eq.8).

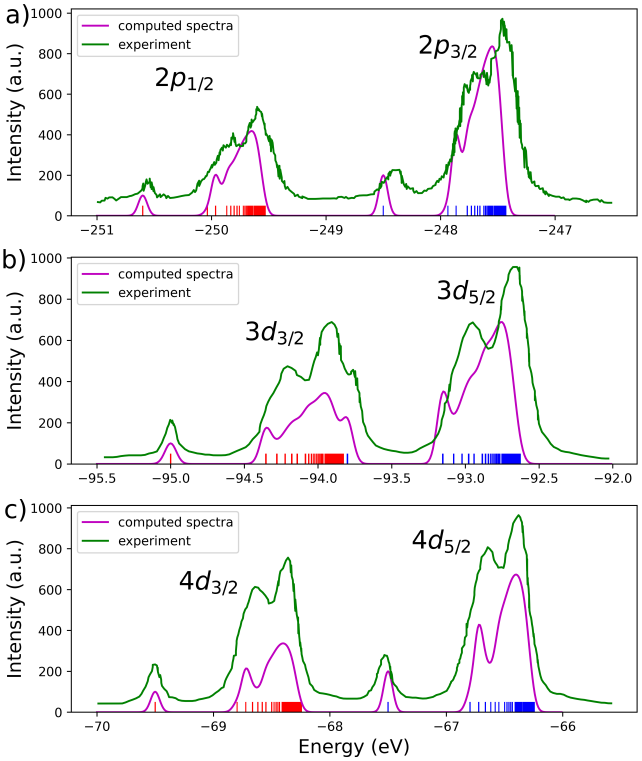


FIG. 3. Simulated and Experimental XPS spectra of a) Ar, b) Kr, and c) Xe cluster around 3000 atoms. Short vertical lines represent binding energy from each atom. A Gaussian boradening of 50meV was used.

dependent polarization energy, allowing the generation of XPS spectra by avoiding thousands of embedded *GW* calculations. The simulated spectra are compared to experiments. The assigned "surface" or "bulk" in the experiment spectra might be ambiguous, as XPS remains a surface technique.

*acknowledgments* Part of the calculations were using the allocation of computational resources from GENCI–IDRIS (Grant 2023-A0130912036). For the purpose of Open Access, a CC-BY public copyright licence has been applied by the authors to the present document and will be applied to all subsequent versions up to the Author Accepted Manuscript arising from this submission.

* valerio.olevano@neel.cnrs.fr
† jing.li@cea.fr

[1] K. Siegbhan *et al.*, *ESCA applied to free molecules* (North-Holland, Amsterdam, 1969).
[2] T. A. Carlson, *Photoelectron and Auger Spectroscopy* (Plenum, New York, 1975).
[3] A. Aarva, V. L. Deringer, S. Sainio, T. Laurila, and M. A. Caro, Chemistry of Materials **31**, 9256–9267 (2019).
[4] I. Mukatayev, B. Sklénard, V. Olevano, and J. Li, Physical Review B **106**, L081125 (2022).
[5] D. Mejia-Rodriguez, A. Kunitsa, E. Aprà, and N. Govind, Journal of Chemical Theory and Computation **17**, 7504–7517 (2021).
[6] J. Li, Y. Jin, P. Rinke, W. Yang, and D. Golze, Journal of Chemical Theory and Computation **18**, 7570–7585 (2022).
[7] L. Galleni, F. S. Sajjadian, T. Conard, D. Escudero, G. Pourtois, and M. J. van Setten, The Journal of Physical Chemistry Letters **13**, 8666–8672 (2022).
[8] I. Mukatayev, F. Moevus, B. Sklénard, V. Olevano, and J. Li, The Journal of Physical Chemistry A **127**, 1642–1648 (2023).
[9] M. Tchaplyguine, R. R. Marinho, M. Gisselbrecht, J. Schulz, N. Mårtensson, S. L. Sorensen, A. Naves de Brito, R. Feifel, G. Öhrwall, M. Lundwall, S. Svensson, and O. Björneholm, J. Chem. Phys. **120**, 345 (2004).
[10] G. D'Avino, L. Muccioli, F. Castet, C. Poelking, D. Andrienko, Z. G. Soos, J. Cornil, and D. Beljonne, Journal of Physics: Condensed Matter **28**, 433002 (2016).
[11] J. Li, G. D'Avino, I. Duchemin, D. Beljonne, and X. Blase, J. Phys. Chem. Lett. **7**, 2814 (2016).
[12] J. Li, G. D'Avino, I. Duchemin, D. Beljonne, and X. Blase, Physical Review B **97**, 035108 (2018).
[13] L. Hedin, Phys. Rev. **139**, A796 (1965).
[14] D. Amblard, G. D'Avino, I. Duchemin, and X. Blase, Physical Review Materials **6**, 064008 (2022).
[15] P. Pollak and F. Weigend, Journal of Chemical Theory and Computation **13**, 3696–3705 (2017).
[16] M. Valiev, E. Bylaska, N. Govind, K. Kowalski, T. Straatsma, H. V. Dam, D. Wang, J. Nieplocha, E. Apra, T. Windus, and W. de Jong, Comput. Phys.

Commun. **181**, 1477 (2010).
[17] X. Blase, C. Attaccalite, and V. Olevano, Phys. Rev. B **83**, 115103 (2011).
[18] D. Jacquemin, I. Duchemin, and X. Blase, J. Chem. Theory Comput. **11**, 3290 (2015).
[19] I. Duchemin, J. Li, and X. Blase, Journal of Chemical Theory and Computation **13**, 1199–1208 (2017).
[20] F. Weigend, Journal of Computational Chemistry **29**, 167–175 (2008).
[21] G. D'Avino, L. Muccioli, C. Zannoni, D. Beljonne, and Z. G. Soos, Journal of Chemical Theory and Computation **10**, 4959 (2014).
[22] R. H. Orcutt and R. H. Cole, The Journal of Chemical Physics **46**, 697 (1967).
[23] T. M. Miller and B. Bederson, in *Advances in Atomic and Molecular Physics* (Elsevier, 1978) pp. 1–55.
[24] D. G. Henshaw, Physical Review **111**, 1470–1475 (1958).
[25] W. H. Keesom and H. H. Mooy, Nature **125**, 889 (1930).
[26] D. R. Sears and H. P. Klug, The Journal of Chemical Physics **37**, 3002–3006 (1962).
[27] W. Lotz, J. Opt. Soc. Am. **60**, 206 (1970).